AIAA 2001-1533

Aeroelastic Stability Of A Soft-Inplane Gimballed Tiltrotor Model In Hover

Mark W. Nixon, Chester W. Langston, Jeffrey D. Singleton
U.S. Army Research Laboratory
Hampton, VA

David J. Piatak, Raymond G. Kvaternik
NASA Langley Research Center
Hampton, VA

Lawrence M. Corso, Ross Brown
Bell Helicopter Textron, Inc.
Fort Worth, TX

AIAA/ASME/ASCE/AHS/ASC Structures, Structural Dynamics and Materials Conference

April 16-19, 2001 / Seattle, WA

AIAA-2001-1533

AEROELASTIC STABILITY OF A SOFT-INPLANE GIMBALLED TILTROTOR MODEL IN HOVER*

Mark W. Nixon, Aerospace Engineer
Chester W. Langston, Aerospace Engineer
Jeffrey D. Singleton, Aerospace Engineer
U.S. Army Vehicle Technology Directorate
Langley Research Center
Hampton, VA

David J. Piatak, Aerospace Technologist
Raymond G. Kvaternik, Senior Research Engineer
NASA Aeroelasticity Branch
Langley Research Center
Hampton, VA

Lawrence M. Corso, Engineer, Rotor Dynamics
Ross Brown, Engineer, Research Projects
Bell Helicopter Textron, Inc.
Fort Worth, TX

ABSTRACT

Soft-inplane rotor systems can significantly reduce the inplane rotor loads generated during the maneuvers of large tiltrotors, thereby reducing the strength requirements and the associated structural weight of the hub. Soft-inplane rotor systems, however, are subject to instabilities associated with ground resonance, and for tiltrotors this instability has increased complexity as compared to a conventional helicopter. Researchers at Langley Research Center and Bell Helicopter-Textron, Inc. have completed an initial study of a soft-inplane gimballed tiltrotor model subject to ground resonance conditions in hover. Parametric variations of the rotor collective pitch and blade root damping, and their associated effects on the model stability were examined. Also considered in the study was the effectiveness of an active swashplate and a generalized predictive control (GPC) algorithm for stability augmentation of the ground resonance conditions. Results of this study show that the ground resonance behavior of a gimballed soft-inplane tiltrotor can be significantly different from that of a classical soft-inplane helicopter rotor. The GPC-based active swashplate was successfully implemented, and served to significantly augment damping of the critical modes to an acceptable value.

 Presented at the 42nd AIAA/ASME/ASCE/AHS/ASC Sturctures, Structural Dynamics, and Materials Conference, Seattle, Washington, April 16-19, 2001.

INTRODUCTION

While three-bladed, gimballed, stiff-inplane rotor systems are employed for the current generation of tiltrotors (XV-15, V-22, BA609), the weight and performance penalties of stiff-inplane rotors may become too significant for use on future systems larger than the V-22. In airplane mode, rotor loads are usually small compared to those in helicopter mode, due to reduced disk loading and axisymmetric inflow conditions. However, during airplane-mode maneuvers such as a rapid pull-up, high oscillatory inplane rotor loads are developed. Tiltrotors employ large highly-twisted blades, creating a significant aerodynamic forcing in the inplane direction where the centrifugal restoring forces are much lower than those associated with the flapping direction. Stiff-inplane hubs must be designed for these inplane loads using additional structure which increases weight and can make the inplane stiffness higher still, leading to more increases in the inplane loads. For larger tiltrotors, this cyclic design challenge can lead to very high structural weights or even to an infeasible design altogether. As a design trade-off, the maximum aerodynamic load capability of a large tiltrotor may be limited to reduce the structural weight of the hub. Such is the case for the V-22 which currently employs a controller to limit the body pitch-rate motion of the aircraft and thereby curtail rotor inplane loads which could otherwise rise above their design allowables (Ref. 1).

Soft-inplane rotor systems can significantly reduce the inplane rotor loads generated during maneuvers of larger tiltrotors, thereby reducing strength re-

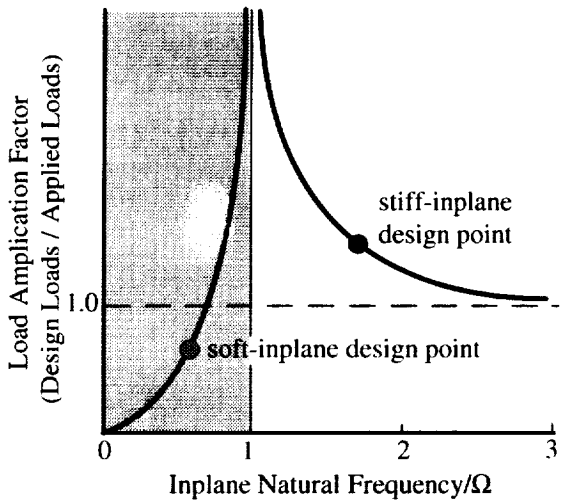

Figur .: Effect of lag frequency on hub loads.

quirements on the hub, leading to reduced structural weight and improved aircraft agility. The plot of Fig. 1 illustrates the benefit with respect to loads for moving from a stiff-inplane design point to a soft-inplane design point. For a soft-inplane rotor system, the lower the inplane natural frequency becomes, the lower the associated hub loads become. The plot also shows that there is a theoretical asymptotic increase in the load factors at 1P due to the resonance of the inplane mode (lead-lag mode) with rotor speed ("lag mode" will be used throughout the remainder of the paper as a description of this mode, however, the terms "inplane" and "lag" will be used interchangeably to be consistent with common usage of the industry). For a soft-inplane rotor system to be effective, it should have a lag frequency below about 0.9/rev, otherwise the loads are about the same as those of the stiff inplane rotor system. A desirable design point for development of a soft-inplane tiltrotor is with a lag frequency of about 0.7/rev (as indicated on Fig. 1). This lag frequency provides a good reduction in design loads and it is about the lowest lag frequency that is practical for the types of soft-inplane hubs currently under consideration for full-scale development. Soft-inplane rotor systems, however, are subject to instabilities associated with ground resonance. Before soft-inplane rotor systems become viable for application to tiltrotors, a comprehensive understanding of the means for avoiding ground resonance instabilities must be established, but there have been few investigations related to this subject to date.

The ground resonance phenomenon is well-understood for conventional helicopters, and the research presented in Refs. 2-10 explain well the phenomenon and characteristics of the onset of ground resonance instabilities. However, there are several differences between helicopters and tiltrotors which suggest that ground resonance behavior of tiltrotors may be significantly different than ground resonance of a helicopter. There is increased complexity for a tiltrotor associated with the participation of elastic wing modes, in addition to the body and rotor modes, which couple through the changing rotor speed during wind-up (start-up). The ground resonance condition is improved with an increase in damping in both the rotor system lag mode and the body or wing mode with which it participates. While the damping of the body modes may be supplemented through mechanical design of the landing gear, there is little that can be adjusted in the elastic modes of a tiltrotor wing without difficulty and significant wing design changes.

The type of hub used for a tiltrotor is another important consideration influencing the characteristics of ground resonance. Previous studies, as is discussed in the review paper of Ref. 10, have considered the important differences between the fully-articulated, hingeless, and bearingless rotor systems with respect to ground resonance on helicopter systems. However, these past efforts may not be applicable to the present effort because none of these conventional hub systems are currently employed on tiltrotors. Standard bearingless rotor systems do not provide enough pitch control for tiltrotor applications while hingeless rotors do not provide enough flap control during differential cyclic maneuvers. Articulated rotor systems are heavier and produce higher drag than the gimballed rotor systems that have become the standard for tiltrotors to date. The current study will focus on the ground resonance behavior of a soft-inplane gimballed rotor system, which may display results significantly different from those associated with the hub systems considered in past studies. However, it should be noted that this type of rotor system may not be feasible for implementation on tiltrotors due to other stability considerations such as high-speed whirlflutter. Although fully-articulated rotors may produce a greater drag penalty in airplane mode, some modification of this hub type may need to be considered to make soft-inplane tiltrotors feasible for all aeroelastic considerations. Additional analysis and testing is required to identify the ideal hub configuration for soft-inplane tiltrotor applications.

To date, the most significant studies of tiltrotor systems subject to ground resonance conditions were made by Boeing Helicopter with the development of their Model 222 tiltrotor concept, a hinge-

less soft-inplane rotor system, which was their entry into a NASA/Army-sponsored tiltrotor research aircraft program (eventually named the XV-15 and won by the Bell Helicopter stiff-inplane rotor system). Ground and air resonance behavior of the Boeing soft-inplane configuration was addressed in several experimental and analytical studies using different size rotor test apparatuses, beginning with a 1/10-scale wind-tunnel model as described in Ref. 11, and ending with a full-scale 26-ft. diameter semispan model tested in the NASA Ames 40- x 80-ft. tunnel as described in Refs. 12 and 13. The Boeing soft-inplane design had a relatively high inplane natural frequency, such that the design rotor speed in hover mode did not create a ground resonance problem. The only experimental results associated with aeromechanical instability of this configuration was obtained with the system in airplane mode subject to air resonance conditions. This configuration was also not gimballed, it was a standard hingeless soft-inplane design. Thus, the tiltrotor configuration of the current study is unique in two important design parameters: 1) the use of a gimbal and constant velocity joint which has a significant effect on the Coriolis forces and therefore the flap-lag blade coupling, and 2) the use of a "low" lag frequency (about 0.5/rev) which creates a resonance condition between the low-frequency lag mode and the critical tiltrotor pylon/wing mode that is well within the design rotor speed envelope. While this latter parameter is not considered a desirable design goal, it does provide some benefits for the current study as shall be discussed.

Researchers at NASA Langley Research Center (LaRC) and Bell Helicopter-Textron, Inc. (BHTI) have completed an initial study of a soft-inplane gimballed tiltrotor model subject to ground resonance conditions in hover. This effort was planned as part of a Memorandum of Agreement between the NASA LaRC and BHTI to "Perform Experimental Aeroelastic Studies of a Tiltrotor Model," and represents the first experiment in a series of tests to be conducted with this soft-inplane hubs on the Wing and Rotor Aeroelastic Testing System (WRATS). The phrase "initial study", as used in the first sentence of this paragraph, indicates that the current hub design is not scaled from a full-scale design that is deemed practical for large scale application. Rather, the current design was developed as a low-cost soft-inplane modification to the existing stiff-inplane gimballed hub representative of the V-22. The objective of the current study was to evaluate the stability characteristics of the gimballed soft-inplane rotor system subject to ground resonance conditions in hover, and also to assess the feasibility of using a generalized predictive controller (GPC) with an active swashplate control system to augment damping and eliminate the ground resonance instabilities. Parametric variations of the rotor collective pitch and blade root damping, and their associated effects on the model stability were also examined in the study.

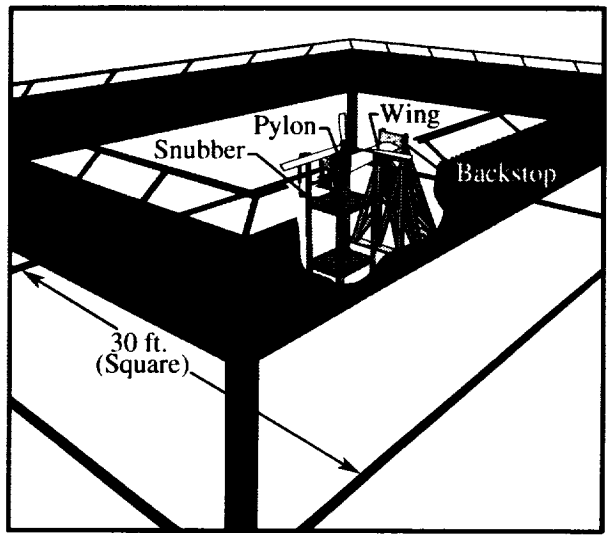

Figure 2: Hover-cell home of the Wing and Rotor Aeroelastic Testing System at the TDT.

APPARATUS

The experimental study was performed in a 30' x 30' hover cell (Fig. 2) located in a high-bay building adjacent to the Transonic Dynamics Tunnel (TDT) at the NASA Langley Research Center in Hampton, Virginia. Notable features of the facility are a backstop mount which centers the tiltrotor model in the hover cell at the same height above the floor as when mounted in the TDT wind-tunnel test section (8 ft.); a snubber stand to halt pylon motion in the advent of an instability; a 3000 psi hydraulic system; 100 psi shop air; 440 volt electric motor power; and a closed-circuit chilled-water system for motor cooling. The model mount was designed to provide stiffness similar to that of the TDT test section sidewall mount so that system frequencies are identical in either the hover or wind-tunnel facilities. Instrumentation wiring runs from the model into an underground cable tray, out of the hover cage, and into a block house control room. Testing is monitored in the control room using a closed-circuit camera system and standard televisions. Signal conditioning, data acquisition equipment and the model pilot control console are located side-by-side in the control room.

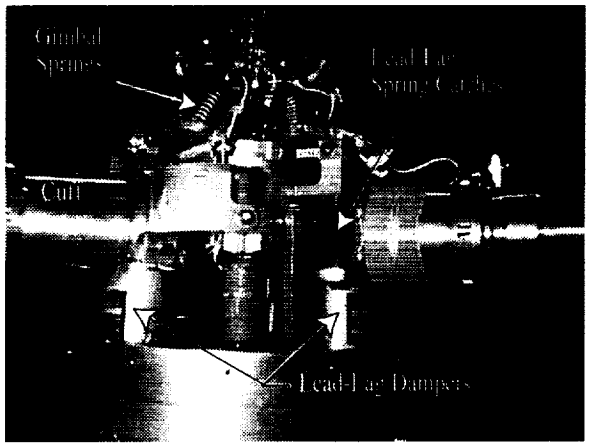

Figure 3: WRATS gimballed soft-inplane parametrically variable hub.

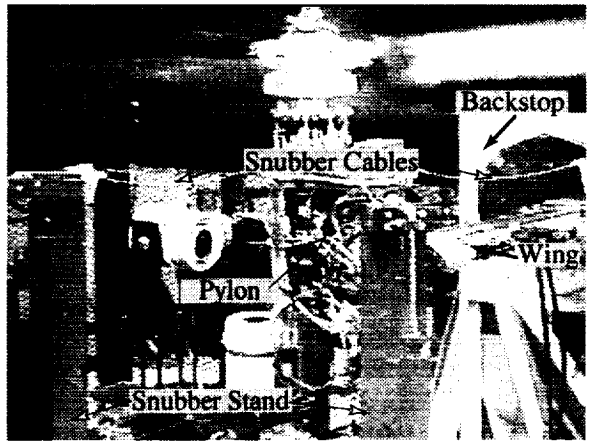

Figure 4: WRATS soft-inplane system in hover.

A remote control unit is used to operate the MG set which controls model rotor speed. It should be noted that while several comparisons between the hover cell and TDT test section were mentioned in this paragraph, the current study was performed entirely in the hover test cell. No wind-tunnel test results have yet been conducted on the soft-inplane version of the tiltrotor model.

The hover test facility described in the previous paragraph was developed in 1995 as a dedicated area for the Wing and Rotor Aeroelastic Testing System (WRATS), a semi-span 1/5-size aeroelastic tiltrotor model based on the V-22. This tiltrotor model has been used in several aeroelastic experimental efforts beginning in 1984 as part of the Navy's JVX program, and more recently has been on loan to NASA LaRC. Since 1994, BHTI and NASA LaRC have had an ongoing cooperative research agreement in place to perform experimental aeroelastic investigations involving the WRATS model with several associated modifications. Some of the more notable investigations include stability augmentation using a composite tailored wing (Ref. 14), vibration reduction using an active flap (Ref. 15), and vibration reduction using an active swashplate (Ref. 16). Important general features of the model are listed as follows: an aeroelastically-scaled wing with removable airfoil panels, a dynamically-scaled pylon with a downstop spring tuned to provide elastic mode shapes and frequencies close to those associated with the full-scale conversion actuator (different springs are used for different conversion actuator positions), a gimballed 3-bladed hub with a constant-velocity joint, and a set of aeroelastically-scaled rotor blades. The current study was performed using the WRATS model, but with the normal stiff-inplane hub modified with the addition of lag hinges to provide a soft-inplane rotor configuration. As illustrated in Fig. 3, the soft-inplane hub is parametrically variable with a set of replaceable coil springs (located behind the lag spring catches) used to tune the lag stiffness, and an adjustable hydraulic damper used to tune the lag damping. The dampers are adjusted by turning a screw which controls the flow of fluid within the damper casing. With the screw open to about 5 turns the damper is ineffective, and only the structural and mechanical damping of the system is present (about 3%). With the screw shut, the damper is almost immovable and the lag motion is critically damped.

Another notable feature of the WRATS tiltrotor model is the hydraulically-controlled swashplate which has high bandwidth controller capability. Three oil cylinder actuators are used to position the swashplate, each controlled by a Moog servo valve using an attached linear variable displacement transducer (LVDT) for position feedback. The pilot control console has three inputs for AC/DC signals (active control commands) which may be summed with the pilot DC input commands and sent to the swashplate control system. The model is shown in Fig. 4 configured for hover testing; and surrounded by the snubber system, but loosely attached to it so that the system properties are not effected.

For testing ground resonance instability, the snubber system provided two benefits. In addition to providing a means for preventing damage to the model with the onset of an instability, it also provided a mechanism for performing isolated rotor testing. While the snubber was activated to restrain the upper portion of the pylon, the lower portion of the pylon could be clamped to the support stand. This

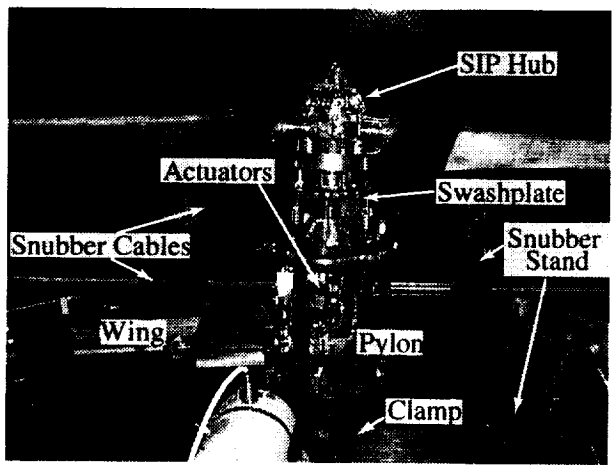

Figure 5: WRATS tiltrotor model setup for isolated rotor testing.

combination would raise the lowest fixed-system frequencies to about 20 Hz. The isolated rotor test setup was used to determine frequencies and damping for the lag mode in the uncoupled system, which are beneficial to know before initiating the part of the experiment where instabilities are likely to occur. A photo of the model setup for isolated rotor testing, with snubber activated and lower pylon clamped to the support stand, is shown in Fig. 5 .

PARAMETRIC STUDY IN HOVER

The stability characteristics of a gimballed soft-inplane tiltrotor model were determined experimentally as a function of collective pitch and lag damper settings for a lag frequency setting of 0.5/rev. The choice of the lag frequency used for the study is a crucial one because it defines the rotor speed at which ground resonance will occur. In general, the lower the lag frequency, the greater the problem with ground resonance instability. While a practical tiltrotor configuration may most likely have a lag frequency of 0.7/rev to 0.8/rev, the current test was developed using a much lower value as indicated. The reason for using 0.5/rev was two-fold: 1) there is a limited number of stock coil springs that could be modified to fit into the spring cage which would produce reasonable lag frequencies, and 2) this value of lag frequency provided instabilities at low rotor speeds so that the ground resonance related characteristics of the system could be fully examined before, during, and beyond the rotor speed at which resonance occurred.

The system frequencies and associated damping were determined experimentally by exciting the pylon with a cyclic stick-stir at the natural frequency of the mode of interest. After removing the excitation, data was processed for approximately 5 seconds, and the frequency and damping were determined using a moving block method (Ref. 17) from the digitized time histories. Obtaining the lag response required slightly more work at some rotor speeds because the response was highly damped and thus did not provide enough cycles outside of the "noise" level to accurately calculate a frequency or damping of the mode. To determine the frequency of the lead lag mode in these instances, the amplitude of the lag response was measured during the excitation produced by the cyclic stick stir. This measurement was repeated for several perturbations of the excitation frequency. When the excitation matched up to the natural frequency of the lag mode then the response amplitude of this mode reached a peak.

The fixed-system mode of interest for the tiltrotor model in hover is best described as a wing torsion/chord coupled elastic mode at approximately 4.9 Hz. For hover, the pylon is oriented vertically above the wing elastic axis creating a significant mass-offset which creates the large coupling between the chord and torsion modes. A second wing mode, beam (vertical) bending, occurs at 5.1 Hz, but since the beam motion is not highly-coupled with the lag rotor motion (the dominant associated pylon motion is perpendicular to the rotor plane), there is a negligible participation of this mode in the ground resonance phenomenon of interest. Also, it should be noted that while in airplane mode the wing beam mode is highly coupled with the wing torsion mode, this is not the case for the hover mode, because of the position of the pylon and the location of its associated mass offset. A third mode at 11.5 Hz is best described as a wing chord/torsion mode, but because of the relatively high frequency, this mode is also insignificant with respect to the ground resonance condition. The 4.9 Hz wing torsion/chord mode (hereafter referred to as WTC) and rotor lag frequencies are shown as a function of rotor speed in Fig. 6 for a condition of 8° collective pitch and damper setting of 3% critical (nonrotating). The plot shows that there is only a slight drop in the wing frequency with rotor speed. The regressive low-frequency lag mode becomes a progressive mode at about 490 RPM. As the rotor speed continues to increase the low-frequency lag mode and the WTC mode become more coupled and the associated frequencies begin to converge.

The damping of these modes is illustrated in the plot of Fig. 7. The plot shows that the lag mode is highly damped, greater than 3% critical except over the rotor speed range where an instability is develop-

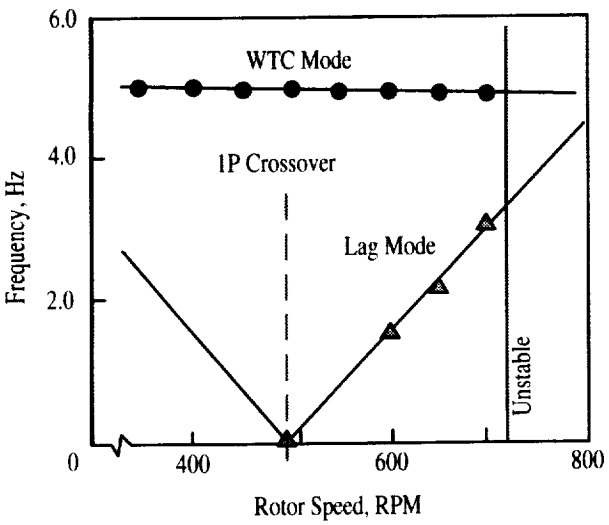

Figure 6: Coupled frequencies of the wing and rotor modes of interest for ground resonance (8° collective and 3% critical lag damper setting).

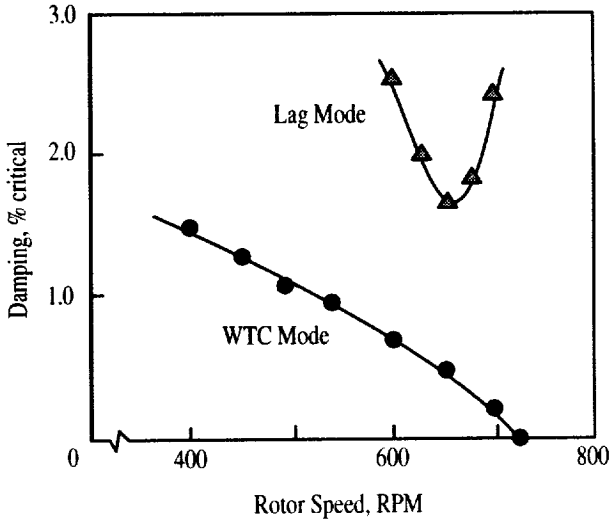

Figure 7: Damping of the wing and rotor modes of interest for ground resonance (8° collective and 3% critical lag damper setting).

ing. Damping at very low rotor speeds could not be measured because there is not sufficient aerodynamic forcing to produce excitations using the stick stirs. The WTC mode damping is shown to decrease at a nearly constant rate with rotor speed, and the mode eventually becomes unstable at about 720 RPM.

The variation of WTC mode damping with rotor speed is shown in Fig. 8 for three collective pitch settings. The results show that the system behavior is extremely sensitive to collective pitch, and this trend is more sensitive than that associated with a typical helicopter system. With an increase in collective pitch, the aerodynamic forces at higher rotor speeds may produce significant hub forces which couple the WTC and blade lag modes, leading to an aeroelastic instability. The WTC mode damping shown in Fig. 8 as a function of rotor speed at the 5° and 12° collective pitch settings also illustrates a trend which is unlike that of classical helicopter ground resonance, but more like a helicopter pylon instability. In classical ground resonance conditions with insufficient rotor lag damping, a sudden and steep reduction followed by a recovery in the lag mode damping is often observed in the vicinity of the resonant frequency. This plot shows that the 5° and 12° collective cases have a relatively slow, but constant, reduction in WTC fixed-system damping as rotor speed increases. Also, following the instability, the WTC mode damping does not recover at higher rotor speeds.

The parametric effect of the damper setting was also considered in this study. Surprisingly, there was little difference in the results of the fixed-system damping and the associated ground resonance instability, even with significant changes in the lag damper setting. In fact, these results are not shown using a plot, as all the curves essentially are overlaid with those shown in Fig. 8. While there is suspicion that these results may be a consequence of the particular design, and that some structural nonlinearities associated with the lag mechanics may play a role in this behavior, this remains a significant and surprising result of the study. It can also be seen that the damper does have an effect on the lag motion itself. The plot of Fig. 9 shows the 1P response of the lag motion as a function of rotor speed, in the vicinity of the lag mode 1P cross-over. The amplitude of the response is shown to be greatly influenced by the damper setting, but this effect does not seem to influence stability of the system.

GENERALIZED PREDICTIVE CONTROL

Control Algorithm

This section describes the theory of GPC in general terms. Implementation of GPC to the specific model used in the study is described in a subsequent section. The essential features of the GPC adaptive control process are depicted in Fig. 10. The system (plant) has r number of control inputs u, m number of measured outputs y, and is subject to unknown external disturbances d. Measurement noise is also present. There are two fundamental steps involved:

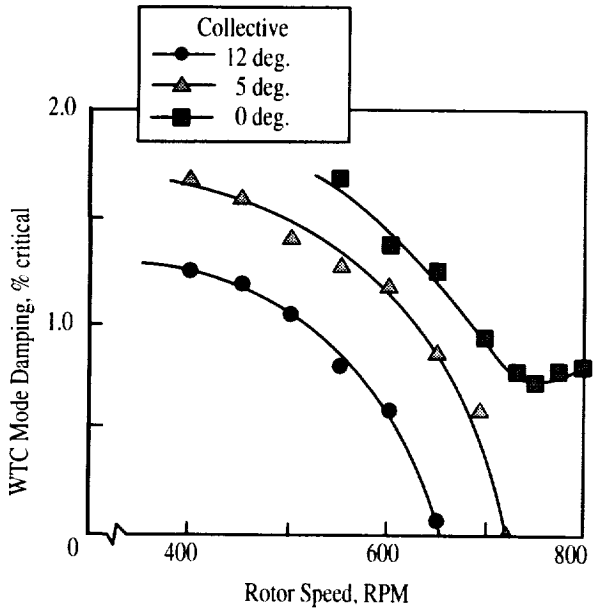

Figure 8: Effect of collective pitch on ground resonance stability with lag damper set to 3% critical.

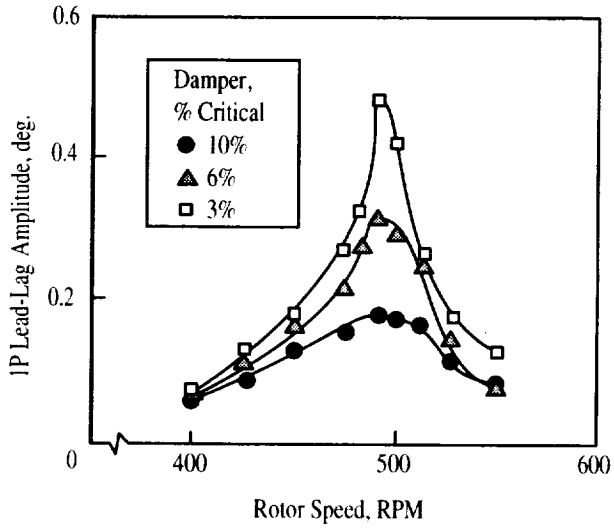

Figure 9: Effect of lag damper on 1P lead-lag response (8° collective).

(1) identification of the system; and (2) use of the identified model to design a controller. A finite-difference model in the form of an auto-regressive moving average with exogenous input (ARX) model is used here. This model is used for both system identification (SID) and controller design. System identification is done on-line in the presence of any disturbances acting on the system, as indicated in the center box of the diagram. In this way, an estimate of the disturbance model is reflected in the identified system model, and does not have to be modeled separately. This approach represents a case of feedback with embedded feedforward. Because the disturbance information is embedded in the feedforward control parameter, there is no need for measurement of the disturbance signal (Ref. 18). The parameters of the identified model are used to compute the predictive control law. A random excitation u_{id} (sometimes called dither) is applied initially with the vector of closed-loop control inputs u_c equal to zero to identify the open-loop system. Dither is added to u_c if it is necessary to re-identify the system while operating in the closed-loop mode.

The relationship between the input and output time histories of a MIMO system are described by the time-domain auto-regressive exogenous (ARX) finite-difference model:

$$y(k) = \alpha_1 y(k-1) + \alpha_2 y(k-2) + ... + \alpha_p y(k-p) + \beta_0 u(k) + \beta_1 u(k-1) + ... + \beta_p u(k-p) \quad (1)$$

This equation states that the current output $y(k)$ at time step k may be estimated by using p sets of the previous output and input measurements, $y(k-1)$, ..., $y(k-p)$ and $u(k-1)$, ..., $u(k-p)$; and the current input measurement $u(k)$. The integer p is called the order of the ARX model. The coefficient matrices α_i and β_i appearing in Eqn. 1 are referred to as observer Markov parameters (OMP), or ARX parameters, and are the quantities to be determined by the identification algorithm.

Closed-loop robustness is enhanced by performing the system identification in the presence of the external disturbances acting on the system, thereby ensuring that disturbance information will be incorporated into the system model. The goal of SID is to determine the OMP based on input and output data. The OMP may be determined by any SID techniques that return an ARX model of the system.

The ARX model is used to design the controller and leads to a control law that in the case of a regulator problem has the general form given by:

$$u_c(k) = \alpha_1^c y(k-1) + \alpha_2^c y(k-2) + ... + \alpha_p^c y(k-p) + \beta_1^c u(k) + \beta_2^c u(k-1) + ... + \beta_p^c u(k-p) \quad (2)$$

This equation indicates that the current control input $u_c(k)$ may be computed using p sets of the previous input and output measurements. The coefficient matrices α_i^c and β_i^c appearing in Eqn. 2 are the control gain matrices.

System identification in the presence of the operation disturbances acting on the system is the first of the two major computational steps. The external disturbances acting on the system are assumed to be unknown (unmeasurable). The number of control inputs is r and the number of measured outputs is m. The system is excited with band-limited white noise for SID. These random excitations are input to all r control inputs simultaneously and the corresponding m responses are measured. The input and output time histories (u and y) are digitized according to the l number of time points, and these parameters are then used to form the data matrices y and V as

$$y = \overline{Y}V \tag{3}$$

where

$$y = [y(0)\ y(1)\ y(2)\ ...\ y(p)\ ...\ y(l-1)] \tag{4}$$

and

$$V = \begin{bmatrix} u(0) & u(1) & u(2) & \dots & u(p) & \dots & u(l-1) \\ & v(0) & v(1) & \dots & v(p-1) & \dots & v(l-2) \\ & & v(0) & \dots & v(p-2) & \dots & v(l-3) \\ & & & \ddots & \vdots & \dots & \vdots \\ & & & & v(0) & \dots & v(l-p-1) \end{bmatrix} \tag{5}$$

The order of the ARX model (p) and the number of time steps (l) must be specified by the user. The size of y is $m \times l$ and the size of V is $[r + (r+m)p] \times l$. Equations 4 and 5 follow from writing the discrete-time state-space equations for a linear time-invariant system at a sequence of time steps $k = 0, l, ..., (l-1)$ and grouping them into matrix form. The vector v is defined as

$$v(k) = \begin{Bmatrix} u(k) \\ y(k) \end{Bmatrix} \tag{6}$$

which has size $(r+m) \times 1$. In forming the matrices of Eqns. 4 and 5, it has been assumed that the state matrix A is asymptotically stable so that for some sufficiently large p, $A^k \approx 0$ for all time steps $k \geq p$, and that an observer has been added to the system. It is through these expedients that the matrix V is reduced to a size amenable for practical numerical computation of its pseudo-inverse. The SID process yields OMP rather than system Markov parameters (SMP) because of the inclusion of an observer. A

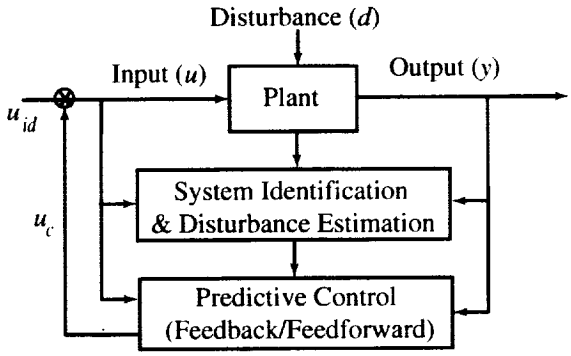

Figure 10: The GPC adaptive control process block diagram.

complete discussion of these aspects of the development may be found in Ref. 19.

$\overline{Y}$ is the matrix of observer Markov parameters which are to be identified and has the form

$$\overline{Y} = \{\, \beta_0\ \beta_1\ \alpha_1\ \beta_2\ \alpha_2\ \beta_3\ \alpha_3\ ...\ \beta_p\ \alpha_p \,\} \tag{7}$$

By solving Eqn. 3 for $\overline{Y}$, the solution may be written as

$$\overline{Y} = yV^{-1} = yV^T[VV^T]^{-1} \tag{8}$$

If the product VV^T is well-conditioned, the ordinary inverse may be taken. Otherwise, a pseudo-inverse must be used. It should be noted that because the size of VV^T is much smaller then V, a pseudo-inverse may be appropriate even if the product is well conditioned.

At this point in the derivation the output prediction equation has been established for one time step. The control law is enhanced by developing the output prediction equation several time steps ahead (multi-step approach). With the α_i and β_i determined by the system identification process, the *multi-step* output prediction equation may be derived at time step $k+j$. Equation 1 may be written at time step $k+j$ as

$$\begin{aligned} y(k+j) = \\ \alpha_1^{(j)}y(k-1) + \alpha_2^{(j)}y(k-2) + ... + \alpha_p^{(j)}y(k-p) \\ + \beta_0 u(k+j) + \beta_0^1 u(k+j-1) + ... + \beta_0^{(j)}u(k) \\ + \beta_1^{(j)}u(k-1) + \beta_2^{(j)}u(k-2) + ... + \beta_p^{(j)}u(k-p) \end{aligned} \tag{9}$$

This equation shows that the output $y(k+j)$ at time step $k+j$ may be estimated by using p sets of the previous output and input measurements, $y(k-1)$, ...,

$y(k-p)$ and $u(k-1)$, ..., $u(k-p)$, and the (unknown) current and future inputs, $u(k)$, $u(k+1)$, ..., $u(k+j)$. The user selects a discrete value for the prediction horizon h_p which provides the range of values for j to be considered. Letting j in Eqn. 9 range over the set of values $j = 1, 2, ..., h_p - 1$, the resulting equations can be assembled into a multi-step output prediction equation:

$$y_{h_p}(k) = Tu_{h_c}(k) + Bu_p(k-p) + Ay_p(k-p) \quad (10)$$

where the coefficient matrices T, B, A are formed from combinations of the observer Markov parameters α_i and β_i. The quantity $y_{h_p}(k)$ is the vector containing the predicted future outputs, whereas $u_{h_c}(k)$ is the vector containing the future control input yet to be determined. The quantities $u_p(k-p)$ and $y_p(k-p)$ are vectors containing the previous p sets of control inputs and outputs, respectively. The vector u_{h_c} in the derivation of Eqn. 10 is originally the size of h_p, but by introducing a new user selectable quantity defined as the control horizon h_c, where $h_c \leq h_p$, the controller performance may be improved. The objective of the controller is now to predict the output for h_p time steps ahead, given the input for h_c steps ahead.

The goal of the GPC algorithm is to determine the set of future commands $u(k)$, $u(k+1)$, ..., $u(k+h_c-1)$ that are required to achieve a desired predicted response $y(k)$, $y(k+1)$, ..., $y(k+h_p-1)$. The multi-step output prediction equation, Eqn. 10, is used to define an objective function whose minimization with respect to $u_{h_c}(k)$ leads to the control law from which a vector of future control inputs can be computed using the p sets of previous control inputs and measured outputs. The predictive control law is obtained by minimizing the deviation of the predicted controlled response (as computed from the multi-step output prediction equation) from a specified target response over a prediction horizon h_p. To this end, an error function ε is defined which is the difference between the desired (target) response $y_T(k)$ and the predicted response $y_{h_p}(k)$:

$$\varepsilon = y_T(k) - y_{h_p}(k) =$$
$$y_T(k) - Tu_{h_c}(k) - Bu_p(k-p) - Ay_p(k-p) \quad (11)$$

An objective function J is then defined which is quadratic in the error ε and in the unknown future controls u_{h_c}:

$$J = \varepsilon^T R\varepsilon + u_{h_c}^T Q u_{h_c} \quad (12)$$

As shown, two weighting matrices are introduced: Q is used to limit the control effort and stabilize the closed-loop system, and R is used to weight the relative importance of the differences between the target and predicted responses. Both matrices are symmetric and positive-semidefinite, and typically are assumed to be diagonal. Also, it is typical in practice for Q to have the same value w_c along its diagonal and for R to have the same value w_r along its diagonal. Minimizing J with respect to $u_{h_c}(k)$ and solving for the same yields:

$$u_{h_c}(k) =$$
$$-(T^T RT + Q)^{-1} \times$$
$$T^T R[-y_T(k) + Bu_p(k-p) + Ay_p(k-p)] \quad (13)$$

which is the control sequence to be applied to the system over the next h_c time steps. The first r values (corresponding to the first future time step) are applied to the r control inputs. The remainder are discarded, and a new control sequence is calculated at the next time step:

$$u_c(k) =$$
$$-\gamma^c y_T(k) + \beta^c u_p(k-p) + \alpha^c y_p(k-p) \quad (14)$$

The target response is zero for a regulator problem and non-zero for a tracking problem. Matrix Q must be tuned to ensure a stable closed-loop system, and typically h_c is chosen equal to h_p. However, h_c may be chosen less than h_p resulting in a more stable, but sluggish, regulator.

GPC Implementation

For the ground resonance investigation, active control of the WRATS tiltrotor model was performed using the high-bandwidth capability (50 Hz) of the swashplate control system (3 hydraulic actuators). The GPC commands were summed at the pilot control console with the pilot input commands before being sent to each of the three actuator control valves. The GPC computations were distributed between two CPUs on a single computer with no user interaction required for data transfer. On user command, data required for system identification was collected on CPU1 and sent to CPU2 where SID was performed and the control gain matrices, α^c and β^c, were computed. The control parameters were automatically sent to CPU1 which used the p latest data sets to compute the control commands (u_c) to be sent to the swashplate actuators. If re-identification was required, the process was repeated on user command. All the algorithms were implemented in dSPACE (a

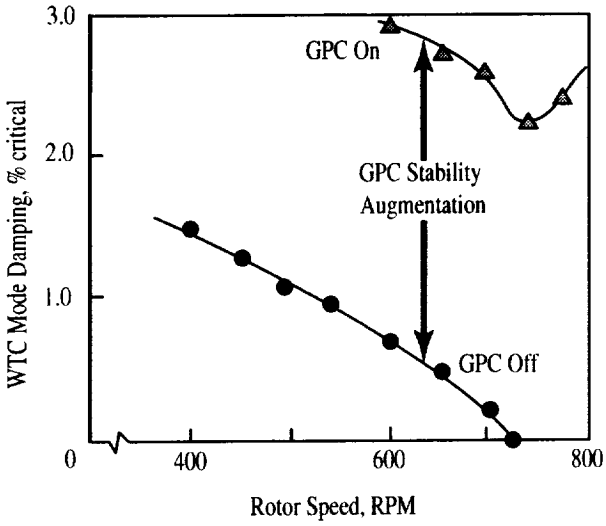

Figure 11: Effect of the GPC controller on ground resonance related damping.

commercially available real-time control system) on a PC with 500 MHz CPUs. The adaptive sequence described in the GPC algorithm section was not included in the current implementation of GPC.

Key results of the investigation are illustrated in the plot of Fig. 11. For the baseline system (GPC off) and a collective pitch setting of 8°, the WTC mode damping is shown to decrease until the model becomes unstable at slightly over 700 RPM. With the GPC control system activated, a large increase in damping was immediately apparent. The plot shows a consistent increase of about 2% critical, and the system did not become unstable within the rotor design speeds considered. Although no results are shown, the vibratory loads associated with the wing modes were examined with GPC both on and off. A reduction in vibratory loads of about 50% was a general rule for the settings on the controller that were optimized for the stability augmentation on the system. It also should be noted that a great deal of work was performed in obtaining the settings (l, p, h_c, h_p, w_c, and w_r) that produced both controller stability and significant damping increases for the model. It was not uncommon during the process of tuning the controller to develop a control instability and then have to shut the control system down and/or snub the model. Once the control settings were established, the performance of the GPC controller were impressive as indicated by Fig. 11.

CONCLUDING REMARKS

With respect to ground resonance behavior, the experimental results obtained for the current test of a gimballed-hub tiltrotor configuration were significantly different than those generally associated with classical helicopter soft-inplane rotor systems. In classical ground resonance conditions with insufficient rotor lag damping, a sudden and steep reduction followed by a recovery in the lag mode damping is often observed in the vicinity of the resonant frequency. The results of the current study show a relatively slow, but constant, reduction in the WTC (critical body mode) damping as rotor speed increases. Also, following the instability, the WTC mode damping does not recover at higher rotor speeds. As there does appear to be an aeroelastic nature to the instabilities in hover, the sensitivity of the instabilities observed to aerodynamic-related design variables such as pitch-flap coupling and pitch-lag coupling will need to be studied further.

Testing of a new generalized predictive control (GPC) system was also completed in this study. The use of GPC with an active swashplate proved to be highly effective at increasing damping and eliminating ground resonance induced instabilities. In addition to increasing the damping, the active control system also reduced vibratory response by about 50% simultaneously. While these results are encouraging, there was some difficulty encountered in determining controller settings that were both effective and stable. The active control implementation used was also not completely automated nor adaptive. Current efforts are focused on improving these aspects of the GPC controller.

REFERENCES

1. Agnihotri, A., Schuessler, W., and Marr, R.: "V-22 Aerodynamic Loads Analysis and Development of Loads Alleviation Flight Control System." Presented at the 45th Annual forum of the American Helicopter Society, Boston, Massachusetts, May 1989.

2. Coleman, R.P. and Feingold, A.M.: "Theory of Self-Excited Mechanical Oscillation of Helicopter Rotors with Hinged Blades." NACA TR-1351, 1956.

3. Lytwyn, R.T., and Miao W.: "Airborne and Ground Resonance of Hingeless Rotors." 26th Annual National Forum of the American Helicopter Society, Washington, D.C., June 1970.

4. Young, M.I., Bailey, D.J., and Murray, S. H.: "Open and Closed Loop Stability of Hingeless Rotor Helicopter Air and Ground Resonance." AHS/NASA-Ames Specialist Meeting on Rotorcraft Dynamics, February 13-15, 1974.

5. Ormiston, Robert A.: "Aeromechanical Stability of Soft Inplane Hingeless Rotor Helicopters." 3rd European Rotorcraft and Powered Lift Aircraft Forum, Aix-En-Provence, France, September 7-9, 1977.

6. Johnson, W.: *Helicopter Theory.* Princeton University Press, Princeton, New Jersey, 1980.

7. Bousman, W.G.: "An Experimental Investigation of the Effects of Aeroelastic Couplings on Aeromechanical Stability of a Hingeless Rotor Helicopter." Journal of the American Helicopter Society, Vol. 26, No. 1, January 1981.

8. Ormiston, Robert A.: "Rotor-Fuselage Dynamic Coupling Characteristics of Helicopter Air and Ground Resonance." Presented at the American Helicopter Society / Nanjing Aeronautical Institute Vertical Flight Technology Seminar, Nanjing, China, November 1985.

9. Yeager, W.T. Jr., Hamouda, M. H., and Mantay, W.R.: "An Experimental Investigation of the Aeromechanical Stability of a Hingeless Rotor in Hover and Forward Flight." NASA TM 89107, AVSCOM TM 87-B-5, June 1987.

10. Chopra, I.: "Perspectives in Aeromechanical Stability of Helicopter Rotors." American Helicopter Society National Specialists' Meeting on Rotorcraft Dynamics, Arlington, Texas, November 13-14, 1989.

11. Alexander, H.R., Hengen, L.H., and Weiberg, J.A.: "Aeroelastic-Stability Characteristics of a V/STOL Tilt-Rotor Aircraft with Hingeless Blades: Correlation of Analysis and Test." 30th Annual Forum of the American Helicopter Society, May 1974.

12. Magee, J.P., Alexander, H.R., Gillmore, K.B., Richardson, D.A., and Peck, W.B..: "Wind Tunnel Tests of a Full Scale Hingeless Prop/Rotor Design for the Boeing Model 222 Tiltrotor Aircraft." Report No. D222-10059-1, Contract NAS2-6505, April 1973.

13. Johnson, W.: "Dynamics of Tilting Proprotor Aircraft in Cruise Flight." NASA TN D-7677, May 1974.

14. Corso, L. M., Popelka, D.A. and Nixon, M. W.: "Design, Analysis, and Test of a Composite Tailored Tiltrotor Wing." Journal of the American Helicopter Society, Volume 45, No. 3, July 2000.

15. Settle, T.B. and Nixon, M.W.: "MAVSS Control of an Active Flaperon for Tiltrotor Vibration Reduction." American Helicopter Society 53rd Annual forum, Virginia Beach, VA, April 29-May 1, 1997.

16. Nixon, M.W., Kvaternik, R.G., and Settle, T.B.: "Tiltrotor Vibration Reduction Through Higher Harmonic Control." Journal of the American Helicopter Society, Volume 43, No. 3, July 1998.

17. Hammond, C.E. and Doggett, R.V. Jr., "Determination of Subcritical Damping by Moving Block/Randomdec Application." NASA Symposium on Flutter Testing Techniques, NASA SP-415, October 1975, pp.59-76.

18. Juang, J.-N. and Eure, K. W.: "Predictive Feedback and Feedforward Control for Systems with Unknown Disturbances." NASA TM-1998-208744, December 1998.

19. Juang, J.-N.: *Applied System Identification.* Prentice Hall, Inc., Englewood Cliffs, New Jersey 07632, 1994, ISBN 0-13-079211-X.